Cavity-enhanced second-harmonic generation via nonlinear-overlap optimization

Citation: Lin, Zin et al. "Cavity-Enhanced Second-Harmonic Generation via Nonlinear-Overlap Optimization." Optica 3.3 (2016): 233.

As Published: http://dx.doi.org/10.1364/optica.3.000233

Publisher: Optical Society of America

Persistent URL: http://hdl.handle.net/1721.1/110204

Version: Original manuscript: author's manuscript prior to formal peer review

Cavity-enhanced second harmonic generation via nonlinear-overlap optimization

Zin Lin[1],* Xiangdong Liang[2], Marko Loncar[1], Steven G. Johnson[2], and Alejandro W. Rodriguez[3]

[1]*School of Engineering and Applied Sciences, Harvard University, Cambridge, MA 02138*

[2]*Department of Mathematics, Massachusetts Institute of Technology, Cambridge, MA 02139 and*

[3]*Department of Electrical Engineering, Princeton University, Princeton, NJ, 08544*

(Dated: May 20, 2015)

Abstract

We describe an approach based on topology optimization that enables automatic discovery of wavelength-scale photonic structures for achieving high-efficiency second-harmonic generation (SHG). A key distinction from previous formulation and designs that seek to maximize Purcell factors at individual frequencies is that our method not only aims to achieve frequency matching (across an entire octave) and large radiative lifetimes, but also optimizes the equally important nonlinear–coupling figure of merit $\bar{\beta}$, involving a complicated spatial overlap-integral between modes. We apply this method to the particular problem of optimizing micropost and grating-slab cavities (one-dimensional multilayered structures) and demonstrate that a variety of material platforms can support modes with the requisite frequencies, large lifetimes $Q > 10^4$, small modal volumes $\sim (\lambda/n)^3$, and extremely large $\bar{\beta} \gtrsim 10^{-2}$, leading to orders of magnitude enhancements in SHG efficiency compared to state of the art photonic designs. Such giant $\bar{\beta}$ alleviate the need for ultra-narrow linewidths and thus pave the way for wavelength-scale SHG devices with faster operating timescales and higher tolerance to fabrication imperfections.

PACS numbers: Valid PACS appear here

Introduction.— Nonlinear optical processes mediated by second-order ($\chi^{(2)}$) nonlinearities play a crucial role in many photonic applications, including ultra-short pulse shaping [1, 2], spectroscopy [3], generation of novel frequencies and states of light [4–6], and quantum information processing [7–9]. Because nonlinearities are generally weak in bulk media, a well-known approach for lowering the power requirements of devices is to enhance nonlinear interactions by employing optical resonators that confine light for long times (dimensionless lifetimes Q) in small volumes V [10–19]. Microcavity resonators designed for on-chip, infrared applications offer some of the smallest confinement factors available, but their implementation in practical devices has been largely hampered by the difficult task of identifying wavelength-scale ($V \sim \lambda^3$) structures supporting long-lived, resonant modes at widely separated wavelengths and satisfying rigid frequency-matching and mode-overlap constraints [15, 20].

In this letter, we extend a recently proposed formulation for the scalable topology optimization of microcavities, where every pixel of the geometry is a degree of freedom, to the problem of designing wavelength-scale photonic structures for second harmonic generation (SHG). We apply this approach to obtain novel micropost and grating microcavity designs supporting strongly coupled fundamental and harmonic modes at infrared and visible wavelengths with relatively large lifetimes $Q_1, Q_2 > 10^4$. In contrast to recently proposed designs based on known, linear cavity structures hand-tailored to maximize the Purcell factors or mode volumes of individual resonances, e.g. ring resonators [17, 21–23] and nanobeam cavities [19, 24], our designs ensure frequency matching and small confinement factors while also simultaneously maximizing the SHG enhancement factor $Q_1^2 Q_2 |\bar{\beta}|^2$ to yield orders of magnitude improvements in the nonlinear coupling $\bar{\beta}$ described by (3) and determined by a special overlap integral between the modes. These particular optimizations of multilayer stacks illustrate the benefits of our formalism in an approachable and experimentally feasible setting, laying the framework for future topology optimization of 2D/3D slab structures that are sure to yield even further improvements.

Structure	$h_x \times h_y \times h_z$ (λ_1^3)	λ (μm)	$(Q_1,\ Q_2)$	$(Q_1^{\text{rad}},\ Q_2^{\text{rad}})$	$\bar{\beta}$	FOM_1	FOM_2
(1) AlGaAs/Al_2O_3 micropost	$8.4 \times 3.5 \times 0.84$	1.5 – 0.75	(5000, 1000)	$(1.4 \times 10^5,\ 1.3 \times 10^5)$	0.018	7.5×10^6	8.3×10^{11}
(2) GaAs gratings in SiO_2	$5.4 \times 3.5 \times 0.60$	1.8 – 0.9	(5000, 1000)	$(5.2 \times 10^4,\ 7100)$	0.020	7×10^6	7.5×10^9
(3) LN gratings in air	$5.4 \times 3.5 \times 0.80$	0.8 – 0.4	(5000, 1000)	(6700, 2400)	0.030	8.4×10^5	9.7×10^7

TABLE I. SHG figures of merit for topology-optimized micropost and grating cavities of different material systems.

Most experimental demonstrations of SHG in chip-based photonic systems [16, 17, 23, 29–32] operate in the so-called small-signal regime of weak nonlinearities, where the lack of pump depletion leads to the well-known quadratic scaling of harmonic output power with incident power [33]. In situations involving all-resonant conversion, where confinement and long interaction times lead to strong nonlinearities and non-negligible down conversion [12, 20], the maximum achievable conversion efficiency $\left(\eta \equiv \frac{P_2^{\text{out}}}{P_1^{\text{in}}}\right)$,

$$\eta^{\text{max}} = \left(1 - \frac{Q_1}{Q_1^{\text{rad}}}\right)\left(1 - \frac{Q_2}{Q_2^{\text{rad}}}\right) \tag{1}$$

occurs at a critical input power [20],

$$P_1^{\text{crit}} = \frac{2\omega_1\epsilon_0\lambda_1^3}{\left(\chi_{\text{eff}}^{(2)}\right)^2|\bar{\beta}|^2Q_1^2Q_2}\left(1 - \frac{Q_1}{Q_1^{\text{rad}}}\right)^{-1}, \tag{2}$$

where $\chi_{\text{eff}}^{(2)}$ is the effective nonlinear susceptibility of the medium [SM], $Q = \left(\frac{1}{Q^{\text{rad}}} + \frac{1}{Q^{\text{c}}}\right)^{-1}$ is the dimensionless quality factor (ignoring material absorption) incorporating radiative decay $\frac{1}{Q^{\text{rad}}}$ and coupling to an input/output channel $\frac{1}{Q^{\text{c}}}$. The dimensionless coupling coefficient $\bar{\beta}$ is given by a complicated, spatial overlap-integral involving the fundamental and harmonic modes [SM],

$$\bar{\beta} = \frac{\int d\mathbf{r}\ \bar{\epsilon}(\mathbf{r})E_2^*E_1^2}{\left(\int d\mathbf{r}\ \epsilon_1|\mathbf{E}_1|^2\right)\left(\sqrt{\int d\mathbf{r}\ \epsilon_2|\mathbf{E}_2|^2}\right)}\sqrt{\lambda_1^3}, \tag{3}$$

where $\bar{\epsilon}(\mathbf{r}) = 1$ inside the nonlinear medium and zero elsewhere. Based on the above expressions one can define the following dimensionless figures of merit,

$$\text{FOM}_1 = Q_1^2Q_2|\bar{\beta}|^2\left(1 - \frac{Q_1}{Q_1^{\text{rad}}}\right)^2\left(1 - \frac{Q_2}{Q_2^{\text{rad}}}\right), \tag{4}$$

$$\text{FOM}_2 = \left(Q_1^{\text{rad}}\right)^2Q_2^{\text{rad}}|\bar{\beta}|^2. \tag{5}$$

where FOM_1 represents the efficiency per power, often quoted in the so-called undepleted regime of low-power conversion [33], and FOM_2 represents limits to power enhancement. Note that for a given radiative loss rate, FOM_1 is maximized when the modes are critically coupled, $Q = \frac{Q^{\text{rad}}}{2}$, with the absolute maximum occurring in the absence of radiative losses, $Q^{\text{rad}} \to \infty$, or equivalently, when FOM_2 is maximized. From either FOM, it is clear that apart from frequency matching and lifetime engineering, the design of optimal SHG cavities rests on achieving a large nonlinear coupling $\bar{\beta}$.

Optimal designs.— Table I characterizes the FOMs of some of our newly discovered microcavity designs, involving simple micropost and gratings structures of various $\chi^{(2)}$ materials, including

GaAs, AlGaAs and $LiNbO_3$. The low-index material layers of the microposts consist of alumina (Al_2O_3), while gratings are embedded in either silica or air (see supplement for detailed specifications). Note that in addition to their performance characteristics, these structures are also significantly different from those obtained by conventional methods in that traditional designs often involve rings [17, 18], periodic structures or tapered defects [24], which tend to ignore or sacrifice $\bar{\beta}$ in favor of increased lifetimes and for which it is also difficult to obtain widely separated modes [19]. Figure 1 illustrates one of the optimized structures—a doubly-resonant rectangular micropost cavity with alternating AlGaAs/Al_2O_3 layers—along with spatial profiles of the fundamental and harmonic modes. It differs from conventional microposts in that it does not consist of periodic bi-layers yet it supports two localized modes at precisely $\lambda_1 = 1.5$ μm and $\lambda_2 = \lambda_1/2$. In addition to having large $Q^{\text{rad}} \gtrsim 10^5$ and small $V \sim (\lambda_1/n)^3$, the structure exhibits an ultra-large nonlinear coupling $\bar{\beta} \approx 0.018$ that is almost an order of magnitude larger than the best overlap found in the literature (see Fig. 2). From an experimental point of view, the micropost system is of particular interest because it can be realized by a combination of existing fabrication techniques such as molecular beam epitaxy, atomic layer deposition, selective oxidation and electron-beam lithography [25]. Additionally, the micropost cavity can be naturally integrated with quantum dots and quantum wells for cavity QED applications [26]. Similar to other wavelength-scale structures, the operational bandwidths of these structures are limited by radiative losses in the lateral direction [10, 25, 27], but their ultra-large overlap factors more than compensate for the increased bandwidth, which ultimately may prove beneficial in experiments subject to fabrication imperfections and for large-bandwidth applications [1, 2, 6, 28].

To understand the mechanism of improvement in $\bar{\beta}$, it is instructive to consider the spatial profiles of interacting modes. Figure 1b plots the y-components of the electric fields in the xz-plane against the background structure. Since $\bar{\beta}$ is a *net* total of positive and negative contributions coming from the local overlap factor $E_1^2 E_2$ in the presence of nonlinearity, not all local contributions are useful for SHG conversion. Most notably, one observes that the positions of negative anti-nodes of E_2 (light red regions) coincide with either the nodes of E_1 or alumina layers (where $\chi^{(2)} = 0$), minimizing negative contributions to the integrated overlap. In other words, improvements in $\bar{\beta}$ do not arise purely due to tight modal confinement but also from the constructive overlap of the modes enabled by the strategic positioning of field extrema along the structure.

Based on the tabulated FOMs (Table I), the efficiencies and power requirements of realistic devices can be directly calculated. For example, assuming $\chi^{(2)}_{\text{eff}}\,(\text{AlGaAs}) \sim 100\ \text{pm/V}$ [18],

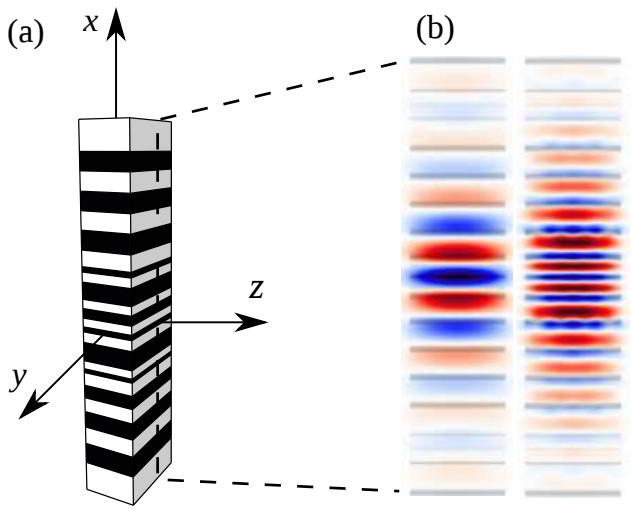

FIG. 1. (a) Schematic illustration of a topology-optimized micropost cavity with alternating AlGaAs/Al_2O_3 layers and dimensions $h_x \times h_y \times h_z = 8.4 \times 3.5 \times 0.84\ (\lambda_1^3)$. For detailed structural specifications, please refer to the supplement. (b) x–z cross-section of the E_y components of two localized modes of frequencies $\lambda_1 = 1.5\mu$m and $\lambda_2 = \lambda_1/2$ and large spatial overlap $\sim E_2^* E_1^2$.

the AlGaAs/Al_2O_3 micropost cavity (Fig. 1) yields an efficiency of $\frac{P_{2,\mathrm{out}}}{P_1^2} = 2.7 \times 10^4/\mathrm{W}$ in the undepleted regime when the modes are critically coupled, $Q = \frac{Q^{\mathrm{rad}}}{2}$. For larger operational bandwidths, e.g. $Q_1 = 5000$ and $Q_2 = 1000$, we find that $\frac{P_{2,\mathrm{out}}}{P_1^2} = 16/\mathrm{W}$. When the system is in the depleted regime and critically coupled, we find that a maximum efficiency of 25% can be achieved at $P_1^{\mathrm{crit}} \approx 0.15\ \mathrm{mW}$ whereas assuming smaller $Q_1 = 5000$ and $Q_2 = 1000$, a maximum efficiency of 96% can be achieved at $P_1^{\mathrm{crit}} \approx 0.96\ \mathrm{W}$.

Comparison against previous designs.— Table II summarizes various performance characteristics, including the aforementioned FOM, for a handful of previously studied geometries with length-scales spanning from mm to a few wavelengths (microns). Fig 2 demonstrates a trend among these geometries towards increasing $\bar{\beta}$ and decreasing Q^{rad} as device sizes decrease. Maximizing $\bar{\beta}$ in millimeter-to-centimeter scale bulky media translates to the well-known problem of phase-matching the momenta or propagation constants of the modes [33]. In this category, traditional WGMRs offer a viable platform for achieving high-efficiency conversion [29]; however, their ultra-large lifetimes (critically dependent upon material-specific polishing techniques), large sizes (millimeter length-scales), and extremely weak nonlinear coupling (large mode volumes) render them far-from optimal chip-scale devices. Although miniature WGMRs such as microdisk and microring resonators [17, 30, 32] show increased promise due to their smaller mode vol-

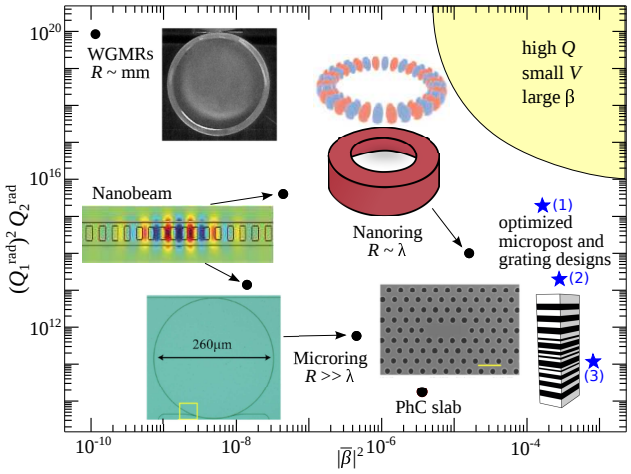

FIG. 2. Scatter plot of $\left(Q_1^{\text{rad}}\right)^2 Q_2^{\text{rad}}$ versus nonlinear overlap $|\bar{\beta}|^2$ for representative geometries, including WGMRs [29], micro- and nano-ring resonators [17, 18], photonic crystal slab and nanobeam cavities [16, 19]. A trend towards decreasing lifetimes and increasing overlaps is readily observed as devices become increasingly smaller. Meanwhile, it remains an open problem to discover structures with high Qs, small Vs and large $|\bar{\beta}|$ (shaded region).

umes, improvements in $\bar{\beta}$ are still hardly sufficient for achieving high efficiencies at low powers. Ultra-compact nanophotonic resonators such as the recently proposed nanorings [18], 2D photonic crystal defects [16], and nanobeam cavities [19], possess even smaller mode volumes but prove challenging for design due to the difficulty of finding well-confined modes at both the fundamental and second harmonic frequencies [16]. Even when two such resonances can be found by fine-tuning a *limited* set of geometric parameters [18, 19], the frequency-matching constraint invariably leads to sub-optimal spatial overlaps which severely limits the maximal achievable $\bar{\beta}$.

Comparing Tables I and II, one observes that for a comparable Q, the topology-optimized structures perform significantly better in both FOM_1 and FOM_2 than any conventional geometry, with the exception of the LN gratings, whose low Q^{rad} lead to slightly lower FOM_2. Generally, the optimized microposts and gratings perform better by virtue of a large and robust $\bar{\beta}$ which, notably, is significantly larger than that of existing designs. Here, we have not included in our comparison those structures which achieve non-negligible SHG by special poling techniques and/or quasi-phase matching methods [32–34], though their performance is still sub-optimal compared to the topology-optimized designs. Such methods are highly material-dependent and are thus not readily applicable to other material platforms; instead, ours is a purely geometrical *topology optimization*

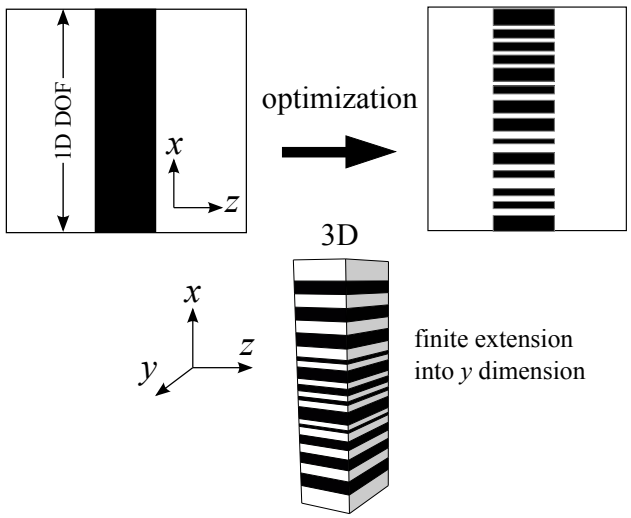

FIG. 3. Work flow of the design process. The degrees of freedom in our problem consist of all the pixels along x-direction in a 2D computational domain. Starting from the vacuum or a uniform slab, the optimization seeks to develop an optimal pattern of material layers (with a fixed thickness in the z-direction) that can tightly confine light at the desired frequencies while ensuring maximal spatial overlap between the confined modes. The developed 2D cross-sectional patterns is truncated at a finite width in the y-direction to produce a fully three-dimensional micropost or grating cavity which is then simulated by FDTD methods to extract the resonant frequencies, quality factors, eigenmodes and corresponding modal overlaps. Here, it must be emphasized that we merely performed one-dimensional optimization (within a 2D computational problem) because of limited computational resources; consequently, our design space is severely constrained.

technique applicable to any material system.

Optimization formulation.— Optimization techniques have been regularly employed by the photonic device community, primarily for fine-tuning the characteristics of a pre-determined geometry; the majority of these techniques involve probabilistic Monte-Carlo algorithms such as particle swarms, simulated annealing and genetic algorithms [35–37]. While some of these *gradient-free* methods have been used to uncover a few unexpected results out of a limited number of degrees of freedom (DOF) [38], *gradient-based* topology optimization methods efficiently handle a far larger design space, typically considering every pixel or voxel as a DOF in an extensive 2D or 3D computational domain, giving rise to novel topologies and geometries that might have been difficult to conceive from conventional intuition alone. The early applications of topology optimization were primarily focused on mechanical problems[39] and only recently have they been expanded to consider photonic systems, though largely limited to *linear* device designs [38, 40–44].

Structure	$\lambda\,(\mu\mathrm{m})$	$(Q_1,\,Q_2)$	$(Q_1^{\mathrm{rad}},\,Q_2^{\mathrm{rad}})$	$\bar{\beta}$	FOM_1	FOM_2
LN WGM resonator [29]	$1.064-0.532$	$(3.4\times10^7$, -)	$(6.8\times10^7$, -)	-	$\sim10^{10}$	-
AlN microring [17]	$1.55-0.775$	$(\sim10^4,\sim5000)$	-	-	2.6×10^5	-
GaP PhC slab [16] *	$1.485-0.742$	(≈ 6000, -)	-	-	$\approx 2\times10^5$	-
GaAs PhC nanobeam [19]	$1.7-0.91^{\dagger}$	(5000, 1000)	($>10^6$, 4000)	0.00021	820	1.8×10^8
	$1.8-0.91$	(5000, 1000)	(6×10^4, 4000)	0.00012	227	2.1×10^5
AlGaAs nanoring [18]	$1.55-0.775$	(5000, 1000)	(10^4, $>10^6$)	0.004	10^5	1.6×10^9

TABLE II. SHG figures of merit, including the frequencies λ, overall and radiative quality factors Q, Q^{rad} and nonlinear coupling $\bar{\beta}$ of the fundamental and harmonic modes, of representative geometries. Also shown are the FOM_1 and FOM_2 figures of merit described in (4), (5).

* SHG occurs between a localized defect mode (at the fundamental frequency) andh an extended index-guided mode of the PhC.

† Resonant frequencies are mismatched.

In what follows, we describe a technique for gradient-based topology optimization of nonlinear wavelength-scale frequency converters.

Recent work [41] considered topology optimization of the cavity Purcell factor by exploiting the concept of local density of states (LDOS). In particular, this previous formulation exploited the equivalency between LDOS and the power radiated by a *point* dipole in order to reduce Purcell-factor maximization problems to a series of small scattering calculations. Defining the objective $\max_{\bar{\epsilon}}\, f\left(\bar{\epsilon}(\mathbf{r});\omega\right) = -\mathrm{Re}[\int d\mathbf{r}\mathbf{J}^*\cdot\mathbf{E}]$, it follows that $\mathbf{E}$ can be found by solving the frequency domain Maxwell's equations $\mathcal{M}\mathbf{E}=i\omega\mathbf{J}$, where $\mathcal{M}$ is the Maxwell operator [SM] and $\mathbf{J}=\delta\left(\mathbf{r}-\mathbf{r}_0\right)\hat{\mathbf{e}}_j$. The maximization is then performed over a finely discretized space defined by the *normalized* dielectric function, $\{\bar{\epsilon}_\alpha=\bar{\epsilon}(\mathbf{r}_\alpha),\ \alpha\leftrightarrow(i\Delta x, j\Delta y, k\Delta z)\}$. A key realization in [41] is that instead of maximizing the LDOS at a single discrete frequency ω, a better-posed problem is that of maximizing the frequency-averaged f in the vicinity of ω, denoted by $\langle f\rangle=\int d\omega'\,\mathcal{W}(\omega';\omega,\Gamma)f(\omega')$, where $\mathcal{W}$ is a weight function defined over some specified bandwidth Γ. Using contour integration techniques, the frequency integral can be conveniently replaced by a single evaluation of f at a complex frequency $\omega+i\Gamma$ [41]. For a fixed Γ, the frequency average effectively shifts the algorithm in favor of minimizing V over maximizing Q; the latter can be enhanced over the course of the optimization by gradually winding down the averaging bandwidth

Γ [41]. A major merit of the frequency-averaged LDOS formulation is that it features a mathematically well-posed objective as opposed to a direct maximization of the cavity Purcell factor $\frac{Q}{V}$, allowing for rapid convergence of the optimization algorithm into an extremal solution.

As suggested in [41], a simple extension of the optimization problem from single- to multi-mode cavities maximizes the minimum of a collection of LDOS at different frequencies. Applying such an approach to the problem of SHG, the optimization objective becomes: $\max_{\bar{\epsilon}_\alpha}\min\Big[\mathrm{LDOS}(\omega_1), \mathrm{LDOS}(2\omega_1)$ which would require solving two *separate* scattering problems, $\mathcal{M}_1\mathbf{E}_1 = \mathbf{J}_1$ and $\mathcal{M}_2\mathbf{E}_2 = \mathbf{J}_2$, for the two distinct *point* sources $\mathbf{J}_1$, $\mathbf{J}_2$ at ω_1 and $\omega_2 = 2\omega_1$ respectively. However, as discussed before, rather than maximizing the Purcell factor at individual resonances, the key to realizing optimal SHG is to maximize the overlap integral $\bar{\beta}$ between $\mathbf{E}_1$ and $\mathbf{E}_2$, described by (3). Here, we suggest an elegant way to incorporate $\bar{\beta}$ by *coupling* the two scattering problems. In particular, we consider not a point dipole but an extended source $\mathbf{J}_2 \sim \mathbf{E}_1^2$ at ω_2 and optimize a single *combined* radiated power $f = -\,\mathrm{Re}\Big[\int d\mathbf{r}\ \mathbf{J}_2^* \cdot \mathbf{E}_2\Big]$ instead of two otherwise *unrelated* LDOS. The advantage of this approach is that f yields precisely the $\bar{\beta}$ parameter along with any resonant enhancement factors ($\sim Q/V$) in $\mathbf{E}_1$ and $\mathbf{E}_2$. Intuitively, $\mathbf{J}_2$ can be thought of as a nonlinear polarization current induced by $\mathbf{E}_1$ in the presence of the second order susceptibility tensor $\boldsymbol{\chi}^{(2)}$, and in particular is given by $J_{2i} = \bar{\epsilon}(\mathbf{r})\sum_{jk}\chi^{(2)}_{ijk}E_{1j}E_{1k}$ where the indices i, j, k run over the Cartesian coordinates. In general, $\chi^{(2)}_{ijk}$ mixes polarizations and hence f is a sum of different contributions from various polarization-combinations. In what follows and for simplicity, we focus on the simplest case in which $\mathbf{E}_1$ and $\mathbf{E}_2$ have the same polarization, corresponding to a diagonal $\boldsymbol{\chi}^{(2)}$ tensor determined by a scalar $\chi^{(2)}_{\mathrm{eff}}$. Such an arrangement can be obtained for example by proper alignment of the crystal orientation axes [SM]. With this simplification, the generalization of the linear topology-optimization problem to the case of SHG becomes:

$$\max_{\bar{\epsilon}_\alpha}\ \langle f(\bar{\epsilon}_\alpha;\omega_1)\rangle = -\mathrm{Re}\Big[\Big\langle \int \mathbf{J}_2^*\cdot\mathbf{E}_2\ d\mathbf{r}\Big\rangle\Big], \tag{6}$$

$$\mathcal{M}_1\mathbf{E}_1 = i\omega_1\mathbf{J}_1,$$

$$\mathcal{M}_2\mathbf{E}_2 = i\omega_2\mathbf{J}_2,\ \omega_2 = 2\omega_1$$

where

$$\mathbf{J}_1 = \delta(\mathbf{r}_\alpha - \mathbf{r}_0)\hat{\mathbf{e}}_j,\ j \in \{x, y, z\}$$
$$\mathbf{J}_2 = \bar{\epsilon}(\mathbf{r}_\alpha)E_{1j}^2\hat{\mathbf{e}}_j,$$
$$\mathcal{M}_l = \nabla \times \frac{1}{\mu}\nabla \times -\epsilon_l(\mathbf{r}_\alpha)\omega_l^2,\ l = 1, 2$$
$$\epsilon_l(\mathbf{r}_\alpha) = \epsilon_{\mathrm{m}} + \bar{\epsilon}_\alpha\ (\epsilon_{\mathrm{d}l} - \epsilon_{\mathrm{m}})\,,\ \bar{\epsilon}_\alpha \in [0, 1],$$

and where ϵ_{d} denotes the dielectric contrast of the nonlinear medium and ϵ_{m} is that of the surrounding linear medium. Note that $\bar{\epsilon}_\alpha$ is allowed to vary continuously between 0 and 1 whereas the intermediate values can be penalized by so-called threshold projection filters [45]. The scattering framework makes it straightforward to calculate the derivatives of f (and possible functional constraints) with respective to $\bar{\epsilon}_\alpha$ via the adjoint variable method [39–41]. The optimization problem can then be solved by any of the many powerful algorithms for convex, conservative, separable approximations, such as the well-known method of moving asymptotes [46].

For computational convenience, the optimization is carried out using a 2D computational cell (in the xz-plane), though the resulting optimized structures are given a finite transverse extension h_y (along the y direction) to make realistic 3D devices (see Fig. 3). In principle, the wider the transverse dimension, the better the cavity quality factors since they are closer to their 2D limit which only consists of radiation loss in the z direction; however, as h_y increases, $\bar{\beta}$ decreases due to increasing mode volumes. In practice, we chose h_y on the order of a few vacuum wavelengths so as not to greatly compromise either Q or $\bar{\beta}$. We then analyze the 3D structures via rigorous FDTD simulations to determine the resonant lifetimes and modal overlaps. By virtue of our optimization scheme, we invariably find that frequency matching is satisfied to within the mode linewidths. We note that our optimization method seeks to maximize the *intrinsic* geometric parameters such as Q^{rad} and $\bar{\beta}$ of an *un-loaded* cavity whereas the *loaded* cavity lifetime Q depends on the choice of coupling mechanism, e.g. free-space, fiber, or waveguide coupling, and is therefore an external parameter that can be considered independently of the optimization. When evaluating the performance characteristics such as FOM_1, we assume total operational lifetimes $Q_1 = 5000,\ Q_2 = 1000$. In the optimized structures, it is interesting to note the appearance of deeply sub-wavelength features $\sim 1 - 5\%$ of $\frac{\lambda_1}{n}$, creating a kind of *metamaterial* in the optimization direction; these arise during the optimization process regardless of starting conditions due to the low-dimensionality of the problem. We find that these features are not easily removable as

their absence greatly perturbs the quality factors and frequency matching.

Concluding remarks.— We have presented a formulation that allows for large-scale optimization of SHG. Applied to simple micropost and grating structures, our approach yields new classes of microcavities with stronger performance metrics over existing designs. One potentially challenging aspect for fabrication in the case of gratings is the presence of deeply sub-wavelength features, which would require difficult high-aspect-ratio etching or growth techniques. This is not an issue for the micropost cavities since each material layer can be grown/deposited to a nearly arbitrary thickness [25, 26]. Another caveat about wavelength-scale cavities is that they are sensitive to structural perturbations near the cavity center, where most of the field resides. In our optimized structures, the figures of merit are robust to within $\sim \pm 20\ \mathrm{nm}$ variations (approximately one computational pixel). One possible way to constrain the optimization to ensure some minimum spatial feature and robustness is to exploit so-called regularization filters and worst-case optimization techniques [45], which we will consider in future work.

Our results provide just a glimpse of the kinds of designs that could be realized in structures with 2D and 3D variations, where we expect even better performance metrics due to the larger design space. In fact, preliminary application of our formulation to 2D systems reveals overlap factors and lifetimes at least one order of magnitude larger than those attained here. Apart from SHG optimization, our approach can be generalized to consider other nonlinear processes, even those involving more than two frequencies [SM]. Preliminary investigations reveal orders-of-magnitude improvements in the efficiency of third harmonic and sum-frequency generation processes. These findings, together with higher-dimensional applications, will be presented in future work.

* zlin@seas.harvard.edu

[1] K. W. DeLong, Rick Trebino, J. Hunter, and W. E. White. Frequency-resolved optical gating with the use of second-harmonic generation. *J. Opt. Soc. Am. B*, 11:2206–2215, 1994.

[2] M. A. Arbore, A. Galvanauskas, D. Harter, M. H. Chou, and M. M. Fejer. Engineerable compression of ultrashort pulses by use of second-harmonic generation in chirped-period-poled lithium niobate. *Opt. Lett.*, 22:1341–1343, 1997.

[3] T. F. Heinz, C. K. Chen, D. Ricard, and Y. R. Shen. Spectroscopy of molecular monolayers by resonant second-harmonic generation. *Phys. Rev. Lett.*, 48:478, 1982.

[4] P. S. Kuo, K. L. Vodopyanov, M. M. Fejer, D. M. Simanovskii, X. Yu, J. S. Harris, D. Bliss, and D.Weyburne. Optical parametric generation of a mid-infrared continuum in orientation-patterned gaas. *Opt. Lett.*, 31:71–73, 2006.

[5] K. L. Vodopyanov, M. M. Fejer, X. Yu, J. S. Harris, Y.-S. Lee, W. C. Hurlbut, V. G. Kozlov, D. Bliss, and C. Lynch. Terahertz-wave generation in quasi-phase-matched gaas. *Appl. Phys. Lett.*, 89:141119, 2006.

[6] Roland Krischek, Witlef Wieczorek, Akira Ozawa, Nikolai Kiesel, Patrick Michelberger, Thomas Udem, and Harald Weinfurter. Ultraviolet enhancement cavity for ultrafast nonlinear optics and high-rate multiphoton entanglement experiments. *Nature Photonics*, 4:170–173, 2010.

[7] Alipasha Vaziri, Gregor Weihs, and Anton Zeilinger. Experimental two-photon, three-dimensional entanglement for quantum communication. *Phys. Rev. Lett.*, 89:240401, Nov 2002.

[8] S. Tanzilli, W. Tittel, M. Halder, O. Alibart, P. Baldi, N. Gisin, and H. Zbinden. A photonic quantum information interface. *Nature*, 437:116–120, 2005.

[9] Sebastian Zaske, Andreas Lenhard, Christian A. Keßler, Jan Kettler, Christian Hepp, Carsten Arend, Roland Albrecht, Wolfgang-Michael Schulz, Michael Jetter, Peter Michler, and Christoph Becher. Visible-to-telecom quantum frequency conversion of light from a single quantum emitter. *Phys. Rev. Lett.*, 109:147404, Oct 2012.

[10] John D. Joannopoulos, Steven G. Johnson, Joshua N. Winn, and Robert D. Meade. *Photonic Crystals: Molding the Flow of Light*. Princeton University Press, second edition, February 2008.

[11] Marin Soljačić, Mihai Ibanescu, Steven G. Johnson, Yoel Fink, and J. D. Joannopoulos. Optimal bistable switching in non-linear photonic crystals. *Phys. Rev. E Rapid Commun.*, 66:055601(R), 2002.

[12] Marin Soljacic, C. Luo, J. D. Joannopoulos, and S. Fan. Nonlinear photonic crystal microdevices for optical integration. *Opt. Lett.*, 28:637–639, 2003.

[13] M. F. Yanik, S. Fan, and M. Soljacic. High-contrast all-optical bistable switching in photonic crystal microcavities. *Appl. Phys. Lett.*, 83:2739–2741, 2003.

[14] Mehmet F. Yanik, Shanhui Fan, Marin Soljačić, , J. D. Joannopoulos, and Yanik. All-optical transistor action with bistable switching in a photonic crystal cross-waveguide geometry. *Opt. Lett.*, 68:2506, 2004.

[15] J. Bravo-Abad, A. W. Rodriguez, J. D. Joannopoulos, P. T. Rakich, S. G. Johnson, and M. Soljacic. Efficient low-power terahertz generation via on-chip triply-resonant nonlinear frequency mixing. *Appl. Phys. Lett.*, 96:101110, 2010.

[16] Kelley Rivoire, Ziliang Lin, Fariba Hatami, W. Ted Masselink, and Jelena Vučković. Second harmonic generation in gallium phosphide photonic crystal nanocavities with ultralow continuous wave pump power. *Opt. Express*, 17(25):22609–22615, Dec 2009.

[17] W. H. P. Pernice, C. Xiong, C. Schuck, and H. X. Tang. Second harmonic generation in phase matched aluminum nitride waveguides and micro-ring resonators. *Applied Physics Letters*, 100(22), 2012.

[18] Zhuan-Fang Bi, Alejandro W. Rodriguez, Hila Hashemi, David Duchesne, Marko Loncar, Ke-Ming Wang, and Steven G. Johnson. High-efficiency second-harmonic generation in doubly-resonant $\chi(2)$ microring resonators. *Opt. Express*, 20(7):7526–7543, Mar 2012.

[19] Sonia Buckley, Marina Radulaski, Jingyuan Linda Zhang, Jan Petykiewicz, Klaus Biermann, and Jelena Vučković. Multimode nanobeam cavities for nonlinear optics: high quality resonances separated by an octave. *Opt. Express*, 22(22):26498–26509, Nov 2014.

[20] Alejandro Rodriguez, Marin Soljačić, J. D. Joannopulos, and Steven G. Johnson. $\chi^{(2)}$ and $\chi^{(3)}$ harmonic generation at a critical power in inhomogeneous doubly resonant cavities. *Opt. Express*, 15(12):7303–7318, 2007.

[21] Vilson R. Almeida, Carlos A. Barrios, Roberto R. Panepucci, and Michal Lipson. All-optical control of light on a silicon chip. *Nature*, 431:1081–1084, 2004.

[22] Qianfan Xu and Michal Lipson. Carrier-induced optical bistability in silicon ring resonators. *Opt. Lett.*, 31(3):341–343, 2005.

[23] Jacob S. Levy, Mark A. Foster, Alexander L. Gaeta, and Michal Lipson. Harmonic generation in silicon nitride ring resonators. *Opt. Express*, 19(12):11415–11421, 2011.

[24] Parag B. Deotare, Murray W. McCutcheon, Ian W. Frank, Mughees Khan, and Marko Loncar. High quality factor photonic crystal nanobeam cavities. *Appl. Phys. Lett.*, 94:121106, 2009.

[25] Kerry Vahala, editor. *Optical microcavities*. World Scientific, USA, 2004.

[26] M. Lermer, N. Gregersen, F. Dunzer, S. Reitzenstein, S. Hofling, J. Mork, L. Worschech, M. Kamp, and A. Forchel. Bloch-wave engineering of quantum dot micropillars for cavity quantum electrodynamics experiments. *Phys. Rev. Lett.*, 108:057402, 2012.

[27] Yinan Zhang and Marko Loncar. Sub-micron diameter micropillar cavities with high quality factors and ultra-small mode volumes. *arXiv:0902.2553*, 2009.

[28] M. Scalora, M. J. Bloemer, A. S. Manka, J. P. Dowling, C. M. Bowden, R. Viswanathan, and J. W. Haus. Pulsed second-harmonic generation in nonlinear, one-dimensional, periodic structures. *Phys. Rev. A*, 56:3166, 1997.

[29] J. U. Fürst, D. V. Strekalov, D. Elser, M. Lassen, U. L. Andersen, C. Marquardt, and G. Leuchs. Naturally phase-matched second-harmonic generation in a whispering-gallery-mode resonator. *Phys. Rev. Lett.*, 104:153901, Apr 2010.

[30] Severine Diziain, Reinhard Geiss, Matthias Zilk, Frank Schrempel, Ernst-Bernhard Kley, Andreas Tunnermann, and Thomas Pertsch. Second harmonic generation in free-standing lithium niobate photonic crystal l3 cavity. *Applied Physics Letters*, 103(5):051117–051117–4, Jul 2013.

[31] Cheng Wang, Michael J. Burek, Zin Lin, Haig A. Atikian, Vivek Venkataraman, I-Chun Huang, Peter Stark, and Marko Lončar. Integrated high quality factor lithium niobate microdisk resonators. *Opt. Express*, 22(25):30924–30933, Dec 2014.

[32] Kuo P. S., Bravo-Abad J., and Solomon G. S. Second-harmonic generation using quasi-phasematching in a gaas whisphering-gallery-mode microcavity. *Nature Comm.*, 5(3109), 2014.

[33] Robert W. Boyd. *Nonlinear Optics*. Academic Press, California, 1992.

[34] G. D. Miller, R. G. Batchko, W. M. Tulloch, D. R. Weise, M. M. Fejer, and R. L. Byer. 42%-efficient single-pass cw second-harmonic generation in periodically poled lithium niobate. *Opt. Lett.*, 22(24):1834–1836, 1997.

[35] Woo Jun Kim and John D. O'Brien. Optimization of a two-dimensional photonic-crystal waveguide branch by simulated annealing and the finite-element method. *J. Opt. Soc. Am. B*, 21(2):289–295, Feb 2004.

[36] Behnam Saghirzadeh Darki and Nosrat Granpayeh. Improving the performance of a photonic crystal ring-resonator-based channel drop filter using particle swarm optimization method. *Optics Communications*, 283(20):4099 – 4103, 2010.

[37] Momchil Minkov and Vincenzo Savona. Automated optimization of photonic crystal slab cavities. *Sci. Rep.*, 4(10.1038/srep05124), 2014.

[38] Alexander Gondarenko, Stefan Preble, Jacob Robinson, Long Chen, Hod Lipson, and Michal Lipson. Spontaneous emergence of periodic patterns in a biologically inspired simulation of photonic structures. *Phys. Rev. Lett.*, 96:143904, Apr 2006.

[39] Martin Philip Bendose and Ole Sigmund. *Topology optimization*. Springer, USA, 2004.

[40] J.S. Jensen and O. Sigmund. Topology optimization for nano-photonics. *Laser and Photonics Reviews*, 5(2):308–321, 2011.

[41] Xiangdong Liang and Steven G. Johnson. Formulation for scalable optimization of microcavities via the frequency-averaged local density of states. *Opt. Express*, 21(25):30812–30841, Dec 2013.

[42] David Liu, Lucas H. Gabrielli, Michal Lipson, and Steven G. Johnson. Transformation inverse design. *Opt. Express*, 21(12):14223–14243, Jun 2013.

[43] Alexander Y. Piggott, Jesse Lu, Thomas M. Babinec, Konstantinos G. Lagoudakis, Jan Petykiewicz, and Jelena Vuckovic. Inverse design and implementation of a wavelength demultiplexing grating coupler. *Sci. Rep.*, 4(10.1038/srep07210), 2014.

[44] Han Men, Karen Y. K. Lee, Robert M. Freund, Jaime Peraire, and Steven G. Johnson. Robust topology optimization of three-dimensional photonic-crystal band-gap structures. *Optics Express*, 22:22632–22648, September 2014.

[45] Fengwen Wang, BoyanStefanov Lazarov, and Ole Sigmund. On projection methods, convergence and robust formulations in topology optimization. *Structural and Multidisciplinary Optimization*, 43(6):767–784, 2011.

[46] Krister Svanberg. A class of globally convergent optimization methods based on conservative convex separable approximations. *SIAM Journal on Optimization*, pages 555–573, 2002.

Cavity-enhanced second harmonic generation via nonlinear-overlap optimization: Supplementary materials

Zin Lin[1],* Xiangdong Liang[2], Marko Loncar[1], Steven G. Johnson[2], and Alejandro W. Rodriguez[3]

[1]*School of Engineering and Applied Sciences, Harvard University, Cambridge, MA 02138*

[2]*Department of Mathematics, Massachusetts Institute of Technology, Cambridge, MA 02139 and*

[3]*Department of Electrical Engineering, Princeton University, Princeton, NJ, 08544*

(Dated: May 20, 2015)

Abstract

We review the temporal-coupled mode equations describing second harmonic generation in doubly resonant cavities and motivate the dimensionless nonlinear coupling $\bar{\beta}$ described in Eq. 3 of the main text. We provide further details on the topology optimization formulation for second harmonic generation and describe generalizations to other nonlinear processes. Finally, we present more detailed descriptions of the optimized micropost and gratings cavities.

COUPLED-MODE THEORY FOR SECOND HARMONIC GENERATION

The temporal coupled mode equations describing second harmonic generation (SHG) in a doubly-resonant cavity coupled to a channel are [1]:

$$\frac{da_1}{dt} = i\omega_1\left(1+\frac{i}{2Q_1}\right)a_1 - i\omega_1\beta_1 a_1^* a_2 + \sqrt{\omega_1\left(\frac{1}{Q_1}-\frac{1}{Q_1^{\text{rad}}}\right)}s_{1+}, \tag{1}$$

$$\frac{da_2}{dt} = i\omega_2\left(1+\frac{i}{2Q_2}\right)a_1 - i\omega_2\beta_2 a_1^2, \tag{2}$$

$$s_{1-} = \sqrt{\omega_1\left(\frac{1}{Q_1}-\frac{1}{Q_1^{\text{rad}}}\right)}a_1 - s_{1+}, \tag{3}$$

$$s_{2-} = \sqrt{\omega_2\left(\frac{1}{Q_2}-\frac{1}{Q_2^{\text{rad}}}\right)}a_2 \tag{4}$$

such that $|a_k|^2$ is the modal energy in the cavity and $|s_{k\pm}|^2$ is the input/output power in the waveguide, and where Q_k and Q_k^{rad} denote the total and radiative quality factors corresponding to mode k. The nonlinear coupling coefficient β_1, obtained from perturbation theory [1], is given by:

$$\beta_1 = \frac{1}{4}\frac{\int d\mathbf{r}\ \epsilon_0 \sum_{ijk}\chi^{(2)}_{ijk}(\mathbf{r})\left(E^*_{1i}E_{2j}E^*_{1k}+E^*_{1i}E^*_{1j}E_{2k}\right)}{\left(\int d\mathbf{r}\ \epsilon_0\epsilon_1(\mathbf{r})|\mathbf{E}_1|^2\right)\left(\sqrt{\int d\mathbf{r}\ \epsilon_0\epsilon_2(\mathbf{r})|\mathbf{E}_2|^2}\right)}.$$

with $\beta_2 = \beta_1^*/2$ far off from material resonances where Kleinman symmetry is valid [2], as required by conservation of energy [1]. In general, the overlap integral in the numerator is a sum of products between different E-field polarizations weighted by off-diagonal components of the nonlinear $\chi^{(2)}$ tensor. For simplicity, however, in the main text we only consider the simple case of diagonal $\chi^{(2)}$ involving same–polarization interactions described by an effective $\chi^{(2)}_{\text{eff}}$, resulting from an appropriate orientation of the crystal axes of the nonlinear material. All of these considerations suggest a simple dimensionless normalization of β, given by:

$$\bar{\beta} = \frac{\int d\mathbf{r}\ \bar{\epsilon}(\mathbf{r})E_2^*E_1^2}{\left(\int d\mathbf{r}\ \epsilon_1|\mathbf{E}_1|^2\right)\left(\sqrt{\int d\mathbf{r}\ \epsilon_2|\mathbf{E}_2|^2}\right)}\sqrt{\lambda_1^3}, \tag{5}$$

such that $\beta_2 = 4\bar{\beta}\chi^{(2)}_{\text{eff}}/\sqrt{\epsilon_0\lambda_1^3}$. As defined in the text, $\bar{\epsilon}(\mathbf{r}) = 1$ for nonlinear dielectric and $\bar{\epsilon}(\mathbf{r}) = 0$ for the surrounding linear medium.

Most SHG experiments operate in the small-signal regime of small input powers, leading to negligible down-conversion and pump depletion. Ignoring the down-conversion or β_1 term in

Eq. 1, one obtain the following simple expression for the second harmonic output power:

$$\frac{P_2^{\text{out}}}{\left(P_1^{\text{in}}\right)^2} = \frac{8}{\omega_1}\left(\frac{\chi_{\text{eff}}^{(2)}}{\sqrt{\epsilon_0\lambda_1^3}}\right)^2 Q_1^2 Q_2 |\bar{\beta}|^2 \left(1-\frac{Q_1}{Q_1^{\text{rad}}}\right)^2 \left(1-\frac{Q_2}{Q_2^{\text{rad}}}\right). \tag{6}$$

In the limit of large up-conversion and non-negligible down-conversion, solution of the coupled-mode equations yields the maximum efficiency (defined as $\eta = P_2^{\text{out}}/P_1^{\text{in}}$) and corresponding critical power [1]:

$$\eta^{\text{max}} = \left(1-\frac{Q_1}{Q_1^{\text{rad}}}\right)\left(1-\frac{Q_2}{Q_2^{\text{rad}}}\right), \tag{7}$$

$$P_1^{\text{crit}} = \frac{2\omega_1\epsilon_0\lambda_1^3}{\left(\chi_{\text{eff}}^{(2)}\right)^2}\frac{1}{|\bar{\beta}|^2 Q_1^2 Q_2}\left(1-\frac{Q_1}{Q_1^{\text{rad}}}\right)^{-1}. \tag{8}$$

FORMULATION FOR TOPOLOGY OPTIMIZATION OF ARBITRARY NONLINEAR FREQUENCY CONVERSION PROCESS

Nonlinear frequency conversion processes can be viewed as frequency mixing schemes in which two or more *constituent* photons at a set of frequencies $\{\omega_n\}$ interact to produce an output photon at frequency Ω such that $\Omega = \sum_n c_n\omega_n$, where the photon number coefficients $\{c_n\}$ can be either negative or positive, depending on whether the corresponding photons are created or destroyed in the process. In general, because the optical nonlinear response of materials is a tensor and hence the frequency conversion process mixes different polarizations [2]. However, for notational simplicity, we will describe our optimization problem only for a single component of the susceptibility tensor. If one wishes to consider the full tensorial properties, one can easily add extra optimization terms (weighted by the tensor components) by following the same approach described below.

Given a specific nonlinear tensor component $\chi_{ijk...}$, where $i,j,k,... \in \{x,y,z\}$, mediating an interaction between the polarization components $E_i(\Omega)$ and E_{1j}, E_{2k}, ..., we begin with a collection of point dipole currents, each at the *constituent* frequency $\omega_n,\ n \in \{1,2,...\}$ and positioned at the center of the computational cell $\mathbf{r}'$, such that $\mathbf{J}_n = \hat{\mathbf{e}}_{n\nu}\delta(\mathbf{r}-\mathbf{r}')$, where $\hat{\mathbf{e}}_{n\nu} \in \{\hat{\mathbf{e}}_{1j},\ \hat{\mathbf{e}}_{2k},...\}$ is a polarization vector chosen so as to excite the desired E-field polarization components of the corresponding mode. Given the choice of incident currents $\mathbf{J}_n$, we solve Maxwell's equations to obtain the corresponding *constituent* electric-field response $\mathbf{E}_n$, from which one can construct a nonlinear polarization current $\mathbf{J}(\Omega) = \bar{\epsilon}(\mathbf{r})\prod_n E_{n\nu}^{|c_n|(*)}\hat{\mathbf{e}}_i$, where $E_{n\nu} = \mathbf{E}_n \cdot \hat{\mathbf{e}}_{n\nu}$ and $\mathbf{J}(\Omega)$ has

polarization $\hat{\mathbf{e}}_i$ generally different from the constituent polarizations $\hat{\mathbf{e}}_{n\nu}$. Here, (*) denotes complex conjugation for negative c_n and no conjugation otherwise. Finally, we maximize the radiated power $-\mathrm{Re}\Big[\int \mathbf{J}(\Omega)^* \cdot \mathbf{E}(\Omega)\, d\mathbf{r}\Big]$ from $\mathbf{J}(\Omega)$.

The formulation is now given by:

$$\begin{aligned}
\max_{\bar{\epsilon}} f(\bar{\epsilon};\omega_n) &= -\mathrm{Re}\Big[\int \mathbf{J}(\Omega)^* \cdot \mathbf{E}(\Omega)\, d\mathbf{r}\Big], \\
\mathcal{M}(\bar{\epsilon},\omega_n)\mathbf{E}_n &= i\omega_n \mathbf{J}_n,\ \mathbf{J}_n = \hat{\mathbf{e}}_{n\nu}\delta(\mathbf{r}-\mathbf{r}'), \\
\mathcal{M}(\bar{\epsilon},\Omega)\mathbf{E}(\Omega) &= i\Omega\mathbf{J}(\Omega),\ \mathbf{J}(\Omega) = \bar{\epsilon}\prod_n E_{n\nu}^{|c_n|(*)}\hat{\mathbf{e}}_i, \\
\mathcal{M}(\bar{\epsilon},\omega) &= \nabla\times\frac{1}{\mu}\nabla\times - \epsilon(\mathbf{r})\omega^2, \\
\epsilon(\mathbf{r}) &= \epsilon_{\mathrm{m}} + \bar{\epsilon}\ (\epsilon_{\mathrm{d}} - \epsilon_{\mathrm{m}})\ ,\ \bar{\epsilon}\in[0,1].
\end{aligned} \tag{9}$$

In practice, we maximize a frequency-averaged version of the power output $\langle f(\omega)\rangle$ rather than $f(\omega)$ itself since the latter has poor convergence [3], i.e., we maximize $\langle f\rangle = \int d\omega'\, \mathcal{W}(\omega';\omega,\Gamma) f(\omega')$, where we simply choose the weighting function $\mathcal{W}$ to be a simple lorentzian with the desired resonance ω and a certain linewidth Γ,

$$\mathcal{W}(\omega') = \frac{\Gamma/\pi}{(\omega'-\omega)^2+\Gamma^2} \tag{10}$$

(Note that this linewidth is not necessarily the same as the intrinsic radiative linewidth of the cavity in that Γ is a computational artifice introduced to aid rapid convergence [3].) In Ref. [3], it is shown by means of contour integration that this averaging is equivalent to evaluating f at a complex frequency $f(\omega+i\Gamma)$, also equivalent to adding a uniform loss $i\Gamma/\omega$ to $\mu(\mathbf{r})$ and $\epsilon(\mathbf{r})$. In our implementation of the optimization process, we typically begin with a large Γ which affords rapid convergence to a stable geometry in a few hundred iterations. Γ is then decreased by an order of magnitude every time the optimization converges until $\Gamma \sim 10^{-5}$ at which point the structure settles to within a linewidth Γ of the desired frequencies (perfect frequency matching).

Application of this formulation to the problem of second harmonic generation is straightforward and described in the main text, in which case $\Omega = \omega_2 = 2\omega_1$ and $\mathbf{J}(\Omega) = \mathbf{J}_2 = \bar{\epsilon}(\mathbf{r})\ (\hat{\mathbf{e}}_{1j}\cdot\mathbf{E}_1)^2\hat{\mathbf{e}}_{2i}$. Note that for the structures described in the text, we chose $\hat{\mathbf{e}}_{1j} = \hat{\mathbf{e}}_{2i} = \hat{\mathbf{e}}_y$. In addition to the problem statement of Eq. 9, the optimization algorithm also benefits from gradient information of the objective function, which exploits the adjoint variable method [3–5]. Here, we simply quote the result for the gradient of our SHG objective function (dropping the polarization

index y for simplicity), $\langle f(\bar{\epsilon};\omega_1)\rangle = -\mathrm{Re}\Big[\Big\langle \int \mathbf{J}_2^* \cdot \mathbf{E}_2 \, d\mathbf{r} \Big\rangle\Big]$,

$$\begin{aligned}\frac{\partial\langle f\rangle}{\partial\bar{\epsilon}} = &-\mathrm{Re}\Big[E_2\,(E_1^*)^2 + (\epsilon_{\mathrm{d}1}-\epsilon_{\mathrm{m}})\omega_1^2 u_1^* E_1^* \\ &+ (\epsilon_{\mathrm{d}2}-\epsilon_{\mathrm{m}})\omega_2^2 u_2 E_2 + i\omega_2 u_2 E_1^2 \\ &+ i\omega_2\omega_1^2(\epsilon_{\mathrm{d}1}-\epsilon_{\mathrm{m}})u_3 E_1\Big],\end{aligned}$$

where the functions u_k are solutions of the following scattering problems:

$$\begin{aligned}\mathcal{M}_1 u_1 &= \bar{\epsilon} E_1^* E_2, \\ \mathcal{M}_2 u_2 &= \bar{\epsilon} E_1^2, \\ \mathcal{M}_1 u_3 &= 2\bar{\epsilon} E_1^* u_2.\end{aligned}$$

OPTIMIZED 1D CAVITY DESIGNS

Figure 1 shows the dielectric and E_y field profiles of the three optimized structures, including (a) AlGaAs/Al_2O_3 micropost, (b) GaAs gratings in SiO_2, and (3) LN gratings in air. Along the x cross-section, each computational pixel of thickness Δ represents *either* a high dielectric (nonlinear) or low dielectric (linear) material. For example, in the AlGaAs/Al_2O_3 micropost cavity (assuming $n_1(\mathrm{AlGaAs}) = 3.02$ and $n_2(\mathrm{AlGaAs}) = 3.18$ for AlGaAs with 70% Al [6], and $n(Al_2O_3) = 1.7$), we took $\Delta = 0.015\ \lambda_1$.

* zlin@seas.harvard.edu

[1] Alejandro Rodriguez, Marin Soljačić, J. D. Joannopulos, and Steven G. Johnson. $\chi^{(2)}$ and $\chi^{(3)}$ harmonic generation at a critical power in inhomogeneous doubly resonant cavities. *Opt. Express*, 15(12):7303–7318, 2007.

[2] Robert W. Boyd. *Nonlinear Optics*. Academic Press, California, 1992.

[3] Xiangdong Liang and Steven G. Johnson. Formulation for scalable optimization of microcavities via the frequency-averaged local density of states. *Opt. Express*, 21(25):30812–30841, Dec 2013.

[4] Martin Philip Bendose and Ole Sigmund. *Topology optimization*. Springer, USA, 2004.

[5] J.S. Jensen and O. Sigmund. Topology optimization for nano-photonics. *Laser and Photonics Reviews*, 5(2):308–321, 2011.

[6] Zhuan-Fang Bi, Alejandro W. Rodriguez, Hila Hashemi, David Duchesne, Marko Loncar, Ke-Ming Wang, and Steven G. Johnson. High-efficiency second-harmonic generation in doubly-resonant $\chi(2)$ microring resonators. *Opt. Express*, 20(7):7526–7543, Mar 2012.

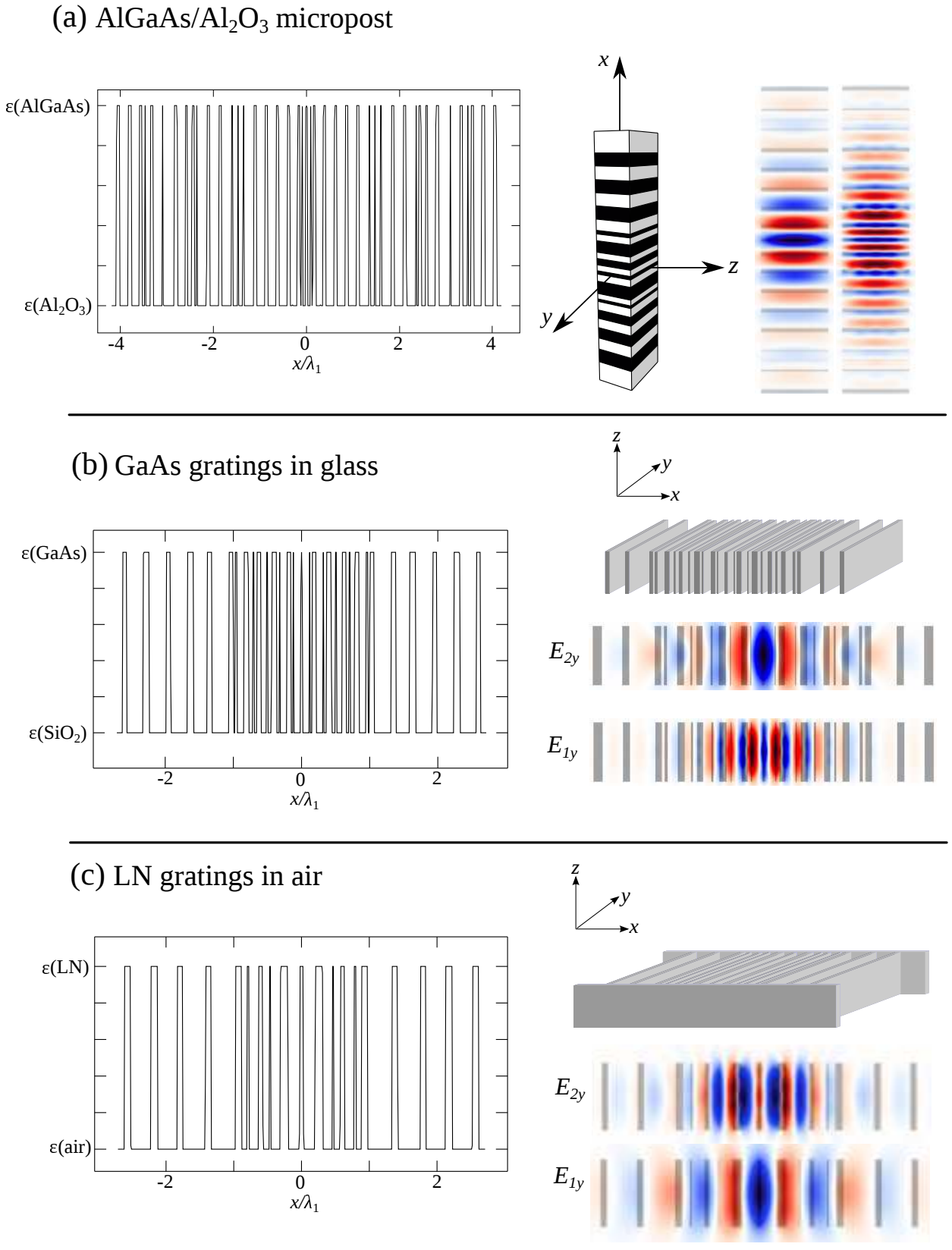

FIG. 1. Cross-sectional dielectric profiles and electric field distributions for AlGaAs/Al_2O_3 micropost (a), GaAs gratings in SiO_2 (b) and LN gratings in air (c).